



COSMIC-RAY MODULATION DUE TO HIGH-SPEED SOLAR-WIND STREAMS OF DIFFERENT SPEED

Dharmendra Singh

Research Scholar

Research center-Govt.Autonomous P.G.College Satna(M.P)

Email- dharmendrasingh738@gmail.com

Dr. P.K. Chamadia

Govt.Autonomous P.G.College Satna (M.P.)

Email - dr.pramod.chamadia @gmail.com

C.M.Tiwari

Department of Physics, APS University Rewa (M.P.)

Email-cmtiwari_2005@yahoo.com

ABSTRACT

This paper puts forward the results of cosmic-ray modulation due to high-speed solar-wind streams of different speed which are identified in the solar wind. The influence of speed of the streams on the Galactic Cosmic ray (GCR) modulation is presented. The relative importance of different solar-wind parameters in the modulation process is also discussed in this paper. This supports the earlier conclusion that the velocity of the stream is not the only parameter that decides the GCR effectiveness of individual HSS. From the averaged time profile of the GCR intensity and solar-wind parameters [V , F , σ_F , E , N , and T], we observed that although after the HSS arrival all these solar-wind parameters increase and reach a maximum level, there are time lags between the maxima of these parameters and minima in GCR intensity; however, this time lag is least with V compared with the other solar-wind parameters [F , σ_F , E , N , and T].

Keywords: Galactic Cosmic ray modulation, solar-wind streams, coronal mass ejections, interplanetary coronal mass ejections and speed.



INTRODUCTION

Observations of solar plasma in space show that the continuous flow of ambient solar wind is frequently covered by faster streams. High-speed solar-wind streams include those released from solar active areas during coronal mass ejections (CMEs) and those ejected from diverging and unipolar-field regions known as coronal holes (CH). As a result, two types of interplanetary structures are associated to two types of magnetic-field topologies on the Sun: interplanetary coronal mass ejections (ICMEs) and corotating interaction regions (CIRs) (Gopalswamy, 2006; Jian et al., 2006a).

Because of the interaction between high-speed CME/CH-streams and ambient solar wind, both ICMEs and CIRs are capable of causing shocks in interplanetary space. Solar-terrestrial interactions caused by interplanetary structures and streams linked with ICMEs and CH have piqued scientists' attention and been intensively researched. Corotating depressions (Sabhah and Kudela, 2011; Modzelevska and Alania, 2012) and Forbush dips in cosmic-ray intensity (Dumbovic et al., 2012; Kumar and Badruddin, 2014a) have received a lot of attention in the past. Long-lived and multiple-step cosmic-ray depressions (Badruddin, 2006) have been reported in ground-based cosmic-ray intensity observations, in addition to solitary Forbush reductions and corotating depressions. As a result, it is critical to look for solar sources, interplanetary causes, and physical mechanisms that are accountable for GCR intensity decreases of varying form, magnitude, and time profile.

The fluctuations in cosmic-ray intensity observed on the ground and in interplanetary space at various time scales are thought to be caused by fields and flows from the Sun. Yet, these flows and fields, particularly those with high speeds ($\geq 400 \text{ kms}^{-1}$) as seen in near-Earth and interplanetary space, have a wide range of speeds reaching up to more than 1000 kms^{-1} . These flows and fields can last anywhere from 2 to 20 days.

Consequently, in this research, we investigate the modification of galactic cosmic rays by high-speed solar-wind streams of varying speeds.

LITERATURE REVIEW

The function of N.M. Wateed et al. (2022) in space weather defines the significance of solar wind research. The solar wind is composed of numerous plasma streams with varied hydrodynamic and magnetic characteristics, as has long been known. Because the distinction between the types of flows is conditional rather than absolute, there is no universally accepted



nomenclature, which differs depending on the author. The number of these types and how they are categorised varies. We looked examined data on solar wind speed and cosmic ray intensity from the National Oceanic and Atmospheric Administration and neutron monitors from 1998 to 2020 for four stations: Apatity, Fort Smith, Hermanus, and Moscow (23, 24, and 25). The three primary types of solar wind include slow and fast wind, as well as disrupted streams. Throughout the research period, the existence of solar wind was detected every day, with low solar wind episodes happening more frequently than fast and disrupted streams.

The unprecedented, uniform, and extensive observations of solar disturbances from space- and ground-based devices, according to Gopalswamy et al (2022), have spurred the expansion of space weather research since the early 1990s. The majority of space weather disruptions are caused by coronal mass ejections (CMEs) from confined magnetic field areas and high-speed streamers (HSS) from open-field zones on the Sun. CMEs and HSS are most notable for their capacity to generate geomagnetic storms and accelerate particles. Particles propelled by CME-driven shocks in space can endanger humans and their technological infrastructure. This review article covers key developments in the knowledge of the relationship between solar variability and space weather.

We offer analysis using daily data gathered from 1995 January to 2018 December by Jacob Oloketuyi et al. (2020). The research was carried out using cross-correlation and wavelet transform methods. The investigations indicated that the intensity of cosmic rays correlates adversely with the number of sunspots, displaying an asynchronous phase connection with a high negative correlation. The trend in cosmic ray intensity reveals that it goes through an 11-year modulation that is mostly determined by solar activity in the heliosphere.

Arvind Dhurve et al. (2019) explored the association between Sunspot number and cosmic ray intensity and discovered that it is negatively related to $r = -0.87$. There is a linear negative relationship between solar wind speed and cosmic ray intensity, with $r = -0.53$. The interplanetary magnetic field (IMF-Bz) displays a substantial negative correlation ($r = -0.90$) with cosmic ray intensity during solar cycles 23 and 24. A minor positive correlation coefficient ($r = 0.19$) was established between the yearly average value of cosmic ray intensity (CRI) and proton density throughout the research period. The solar wind index has an intriguing relationship with the CRI.

Despite a 40% fall in sunspot quantity, Gopalswamy N, et al. (2015) find that halo coronal mass ejections (CMEs) are more abundant in cycle 24 than in cycle 23. We also find



that the distribution of halo-CME source sites changes in cycle 24: the longitude distribution of halos is much flatter, with 600 times as many halos originating at a central meridian distance as in cycle 23. The average speed and magnitude of the associated soft X-ray flare, on the other hand, are the same in both cycles, showing that the ambient medium into which the CMEs are discharged is significantly different. We hypothesize that the higher number and longer central meridian longitudes of halo CMEs in cycle 24 can be explained by a drop in total pressure in the heliosphere. Due of the reduced overall pressure, CMEs may expand more than normal, resulting in halos.

Mittal.N and Narain (2015) showed that the arrival timings of Coronal Mass Ejections (CMEs) near Earth have a significant influence on the solar terrestrial environment. They used LASCO halo CME data from 248 occurrences observed between 1996 and 2007 to predict the arrival times of full halo CMEs as precisely as possible. Different investigations on the arrival timing of halo CMEs associated with type II radio bursts and X-class soft X-ray bursts were carried out. In that investigation, they looked at the location and speed of Earth-directed CMEs. The outcomes of the current investigation are discussed in light of the most recent state of CME knowledge.

The abnormal rise of coronal mass ejections during solar cycle 24 is investigated by Gopalswamy N et al. (2014), as are the consequences for space weather. The well-known relationship between the speed and angular width of coronal mass ejections (CMEs) occurs in solar cycle 24, but the regression line has a steeper slope: CMEs in cycle 24 are much wider than those in cycle 23 for a given CME speed. Due of the low solar activity, the slope change indicates a significant change in the heliosphere's physical state. The entire pressure in the heliosphere (magnetic + plasma) is reduced by ~40%, allowing CMEs to grow abnormally and accounting for the steeper slope. Excessive CME expansion reduces the efficacy of CMEs in generating magnetic storms during cycle 24, both because the magnetic content of the CMEs is diluted and because ambient fields are lower. The reduced magnetic field of the heliosphere may contribute to the absence of solar energetic particles accelerated to very high energy during this cycle.

According to Liou et al. (2014), the July 23, 2012 CME was a very fast backside event, reaching around 1AU (STEREO-A) in 20 hours as compared to 3-6 days for typical CME occurrences. In summary, assuming an initial CME speed of 3100 kms⁻¹, the model findings correlate well with in situ observations in terms of the arrival time of the CME-driven shock



and total magnetic field intensity. According to empirical model extrapolation, the quick CME and its strong magnetic field are capable of creating an unusually big geomagnetic storm, comparable to the well-known Halloween storm of 2003, if the CME made a direct impact on Earth. They looked at the impact of the adiabatic index (γ). It was discovered that for a lower value, the shock arrives somewhat later, γ and $(\gamma) = 5/3$ offers the best agreement for the shock arrival time.

Rahman.A et al. (2013) looked at the stand-off distances of 101 interplanetary CMEs (ICMEs) discovered between 1997 and 2005. The fundamental purpose of this work is to explore the stand-off distance and its link to various CME, ICME, and IP shock features such as Alfvénic Mach numbers and transit time. The relationship between CME speed and stand-off distance found that energetic CMEs had a shorter stand-off distance, implying that the driver CME (the CME that creates the shock) and its shock travel in close proximity. The correlation plot between CME acceleration and stand-off distance revealed that highly decelerated and highly accelerated events had a narrower stand-off distance range (i.e., 10-40 R) than the other events. Stand-off times for events with longer journey lengths to 1 AU (>70h) are 20h, but stand-off times for speedier events with shorter trip times (40h) are extremely low (10h).

DATA ANALYSIS

High-speed solar-wind streams were detected using the OMNI Web data source (omniweb.gsfc.nasa.gov) and tabulated to provide information on some essential aspects of the streams from 1996 to 2007. (Gupta and Badruddin, 2010). We created a catalog for the extended period (2008-2011) using Gupta and Badruddin's criteria (2010). An example compound stream is presented (Figure 1) together with the cosmic-ray intensity fluctuations observed at the Oulu and Hermanus neutron monitors throughout the stream's passage to demonstrate the parameters and symbols of this table. To calculate $\Delta I/I$ [%], plotted in the top two panels, hourly counts were first averaged for the complete plotted period [x]. Then for each hour's count rate [x_i], the value $\{(x_i - x)/x\}$ [%] is calculated and plotted as $\Delta I/I$ [%].

The two catalogs (Gupta and Badruddin (2010) and Table 1) combine to cover the whole solar cycle 23, the deep solar low between solar cycles 23 and 24, and some of the (growing) section of solar cycle 24. We employed these tabular HSS of varying speeds to investigate their efficacy in regulating galactic cosmic rays. The dotted vertical lines on the left

and right represent the stream's start and finish times. We plot the temporal variation of various parameters: GCR-intensity variation recorded by Oulu neutron monitor $[\Delta I/I]_O$ (%), and Hermanus neutron monitor $[\Delta I/I]_H$ (%), the solar-wind velocity $[V, \text{kms}^{-1}]$, plasma density $[N, n \text{ cm}^{-3}]$, plasma temperature $[T, 10^5 \text{ K}]$, interplanetary magnetic field $[B, \text{nT}]$, standard deviation in field vector $[\sigma_F, \text{nT}]$, and the electric field $[E, \text{mV m}^{-1}]$ from 15 July 2010 to 14 August 2010.

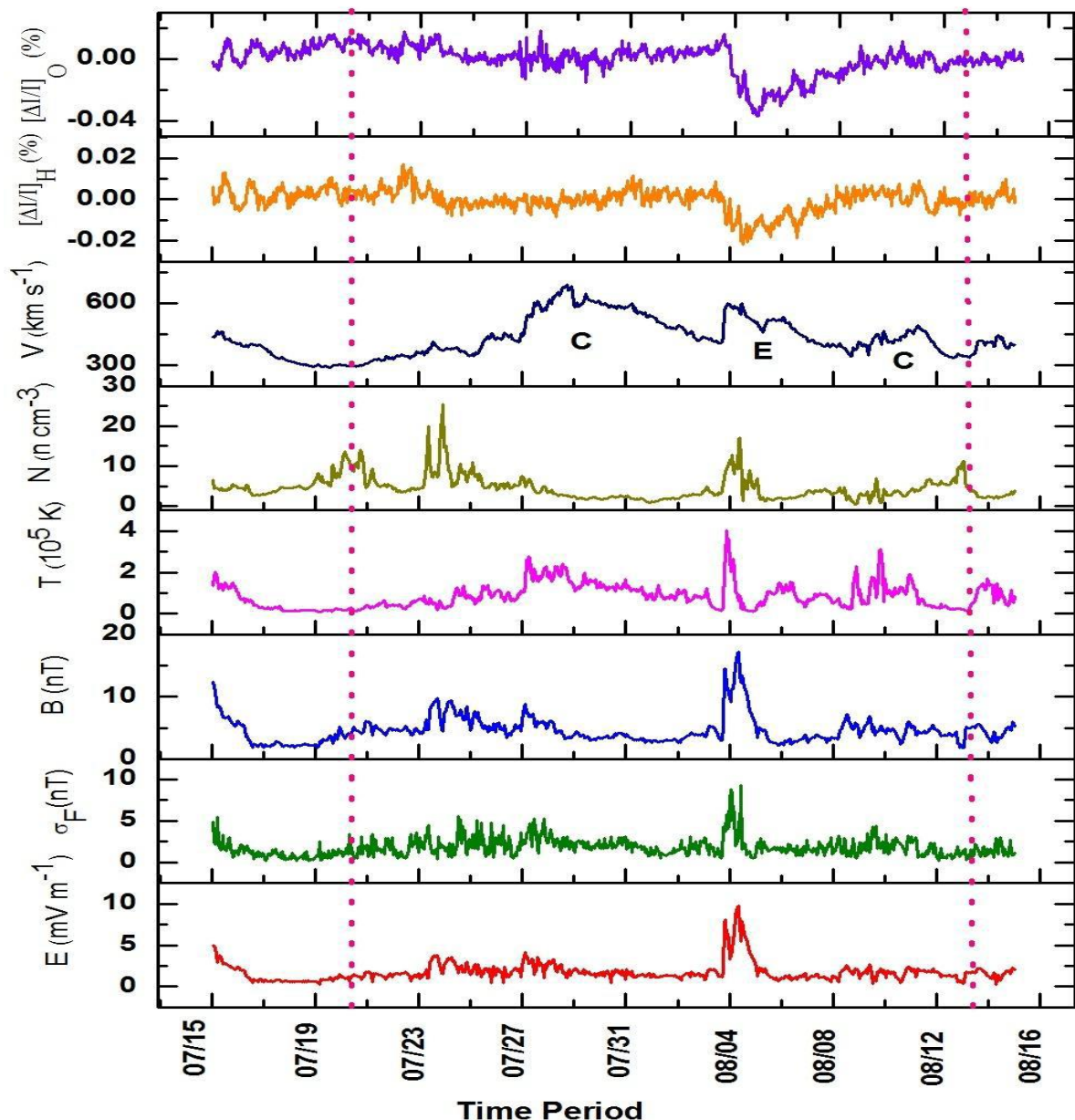


Figure 1 A typical compound high-speed stream caused by two coronal-hole associated streams (C) and a CME associated stream (E) observed between UT: 14:00, 20 July 2010 to UT 14:00, 12 August 2010.



RESULTS AND DISCUSSION

The velocity of high-speed streams in the solar wind detected in near-Earth space range from $\approx 400 \text{ kms}^{-1}$ to 1000 kms^{-1} . To investigate the usefulness of HSS with such a broad speed range in regulating GCR intensity, we separated them into five groups of streams with varying velocity ranges:

- $400 - 500 \text{ kms}^{-1}$,
- $501 - 550 \text{ kms}^{-1}$,
- $551 - 600 \text{ kms}^{-1}$,
- $601 - 650 \text{ kms}^{-1}$,
- $> 650 \text{ kms}^{-1}$.

Observations show that during the passage of the HSS, the density [N] and temperature [T] of the solar-wind plasma also change. Thus these parameters [N and T] together with velocity [V] describe the physical conditions of solar-wind plasma during the passage of the HSS. We also considered the magnitude of magnetic-field vector [F , nT] attributable to the solar-wind plasma, fluctuations/turbulence in the field as indicated by standard deviations in magnetic field [σF , nT], and the interplanetary electric field [$E = FV$, mV m^{-1}] in addition to the solar-wind velocity [V , kms^{-1}] to study the GCR intensity modulation during the passage of the HSS.

To study of the effect of HSS-speed on the GCR-intensity modulation we performed a superposed-epoch analysis of hourly GCR intensity data as observed by neutron monitors: Oulu (Latitude = 64.05 N , Longitude = 25.47 E , cut-off rigidity $R_c = 0.81 \text{ GV}$) and Hermanus (Latitude = 34.42 S , Longitude = 19.23 E , cut-off rigidity $R_c = 4.58 \text{ GV}$) with different cut-off rigidities. Data from two neutron monitors were utilized to demonstrate that the observed fluctuations are not local but worldwide, of comparable type but differing in magnitude because to the two sites' varied cut-off stiffness.

This analysis was performed for the arrival of HSS. The arrival time of the HSS is considered as the epoch (zero hour) for the analysis. The hourly data of neutron monitors, solar-wind velocity [V], interplanetary magnetic-field vector [F], standard deviation of vector magnetic field [σF], interplanetary electric field [E], solar-wind plasma density [N], and temperature [T] were analyzed. The results of the analysis showing the average behavior for

the five speed-groups of the HSS are plotted in Figure 2. The influence of the HSS on GCR intensity is apparent because the intensity begins to decrease upon the arrival of the HSS. Although the temporal variations of GCR intensity correspond to temporal variations of the HSS speed, other solar-wind parameters (*e.g.* magnetic-field vector [F], field fluctuations represented by σF , and interplanetary electric field [E]) are also enhanced at the HSS arrival.

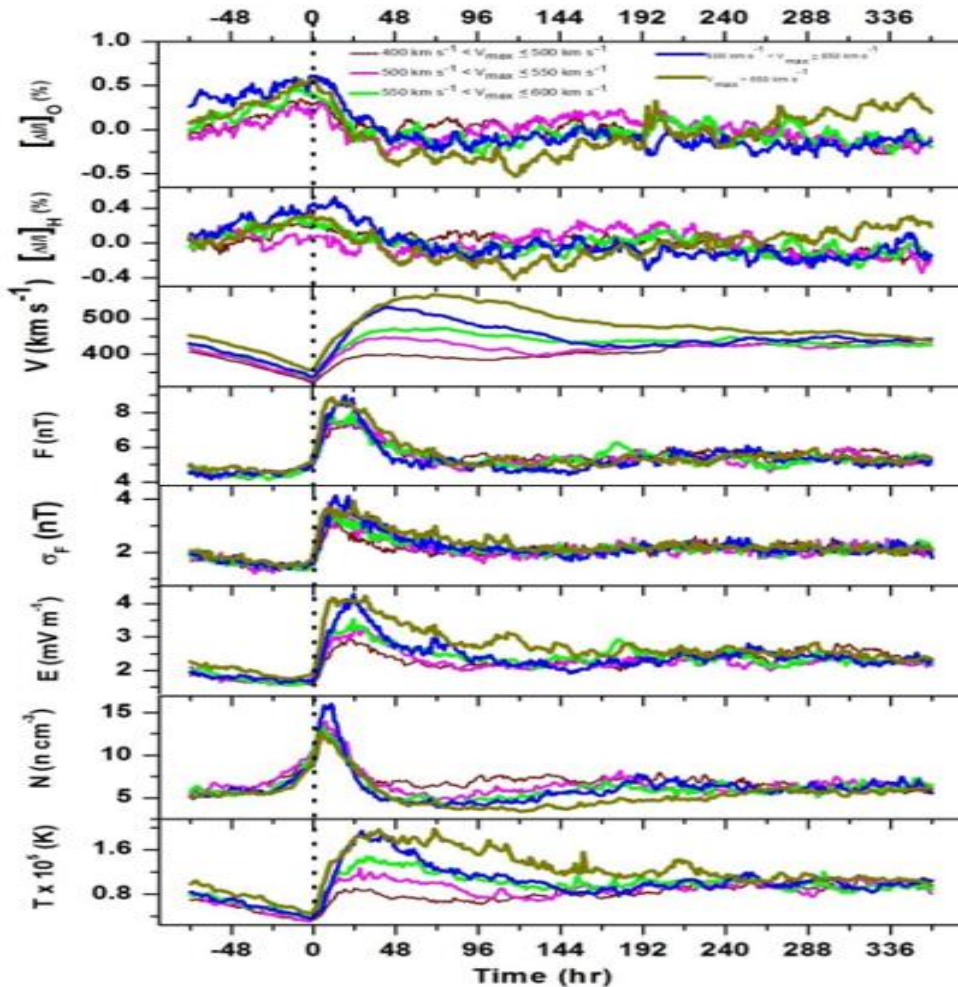


Figure 2 Superposed-epoch analysis results of the GCR-intensity variation recorded at Oulu NM $[\Delta I/I]_O$ (%), at Hermanus NM $[\Delta I/I]_H$ (%) plotted for the arrival times of high-speed streams (zero hour) of the five categories based on the speed

Figure 2 depicts the average behavior, including both temporal fluctuations and parameter amplitudes, throughout the passage of the five HSS speed-groups. These findings, however, show that the GCR efficacy (ability to reduce GCR intensity) of the five HSS speed-groups varies. To investigate the GCR efficacy of HSS further, we measured the magnitude of the GCR-intensity depression generated by each HSS. Then, adopting the criteria suggested by



Kumar and Badruddin (2014a), we divided the GCR effectiveness into four groups, based on certain ranges of the GCR-intensity depressions. These GCR-effective groups are the so-called small (0.01 – 0.49 %), moderate (0.50 – 1.49 %), large (1.50 – 2.99 %), and very large (≥ 3.00 %) depressions, as observed at a mid-latitude neutron monitor. With this division of the GCR effectiveness into four categories, we made a comparative study of the GCR effectiveness of five HSS speed-groups.

The normal temporal profile of each HSS speed-group, as shown in the superposed-epoch plots in Figure 2, is such that the solar-wind velocity begins to climb at zero hour, achieves a maximum speed after a given period, and then begins to progressively drop. Although the temporal profiles are different, the enhancements in other solar-wind parameters [F , σF , E , N , and T] also start near the zero hour, reach a maximum, and then decrease.

Table 1 A catalog of high-speed solar wind streams observed during 2008 – 2011

SN	Year	Start time DD/MM/HH	End time DD/MM/HH	V_{max} [kms ⁻¹] (f)	N_{max} [ncm ⁻³] (g)	T_{max} [10 ⁵ K] (h)	B_{max} [nT] (i)
1	08	05 Jan:00	12 Jan:05	706	40.7	4.09	15.9
2	08	12 Jan:06	24 Jan:11	710	13.0	2.92	9.1
3	08	24 Jan:13	27 Jan:12	550	09.6	2.74	8.9
4	08	31 Jan:08	07 Feb:02	640	34.6	2.25	11.7
5	08	07 Feb:10	09 Feb:02	437	10.4	0.94	8.7
6	08	09 Feb:03	27 Feb:12	725	23.2	3.81	16.9
7	08	27 Feb:13	07 Mar:21	768	21.1	5.28	10.5
8	08	07 Mar:22	26 Mar: 00	701	32.6	4.04	15.9
9	08	26 Mar:01	02 Apr:16	676	23.5	3.56	9.5
10	08	02 Apr:17	16 Apr: 00	738	9.8	3.67	12.2
11	08	16 Apr:01	22 Apr:12	600	15.8	2.65	10.5
12	08	22 Apr: 13	30 Apr:15	654	17.6	5.22	11.8
13	08	30 Apr: 16	10 Apr:00	642	26.1	2.26	8.3
14	08	18 May:03	28 May:00	593	26.7	2.96	8.4
15	08	28 May:01	06 Jun:03	632	35.2	5.02	9.7
16	08	06 Jun:04	14 Jun:11	514	16.8	1.96	8.0
17	08	14 Jun:12	24 Jun:14	754	37.9	4.97	14.8
18	08	24 Jun:15	04 Jul:08	641	19.8	3.20	13.4
19	08	04 Jul:09	09 Jul:01	413	17.4	1.54	9.1
20	08	09 Jul:02	20 Jul:11	697	15.5	3.30	14.6
21	08	20 Jul:12	31 Jul:23	663	18.6	3.50	9.7
22	08	08 Aug:06	16 Aug:15	645	30.2	4.68	18.3
23	08	16 Aug:16	24 Aug:10	626	22.9	3.66	9.7
24	08	02 Sep:19	13 Sep:17	622	20.5	2.96	14.8
25	08	14 Sep:04	23 Sep:08	583	39.5	2.86	11.6
26	08	30 Sep:11	08 Oct:19	705	9.9	3.35	8.2
27	08	11 Oct:05	17 Oct:10	548	32.1	3.75	13.5



28	08	28 Oct:01	05 Nov:18	705	15.2	3.60	13.8
29	08	6 Nov:07	14 Nov:12	573	29.1	2.74	11.9
30	08	14 Nov:13	22 Nov:01	517	18.9	1.81	13.5
31	08	24 Nov:23	02 Dec:11	648	74.9	3.89	21.7
32	08	02 Dec:12	21 Dec:19	567	24.4	2.62	10.7
33	08	21 Dec:20	30 Dec:02	556	25.3	2.58	11.5
34	08	31 Dec:03	08 Jan:05	535	19.3	2.49	13.4
35	09	12 Jan:15	23 Jan:08	477	16.9	1.95	12.4
36	09	25 Jan:12	03 Feb:19	496	20.5	2.41	10.6
37	09	13 Feb:20	19 Feb: 05	581	50.7	3.25	15.9
38	09	19 Feb:06	03 Mar:02	679	20.9	3.21	8.6
39	09	10 Mar:09	19 Mar: 13	567	21.9	2.99	18.4
40	09	19 Mar:21	03 Apr:06	489	10.7	1.91	10.1
41	09	03 Apr:07	16 Apr: 09	551	20.7	2.11	8.5
42	09	16 Apr:10	01 May:09	536	27.0	2.02	11.1
43	09	02 May:09	13 May:14	508	16.3	2.02	7.1
44	09	27 May:23	23 Jun:02	434	29.8	1.53	10.1
45	09	24 Jun:02	09 Jul: 11	557	82.5	2.87	13.4
46	09	09 Jul:12	18 Jul: 06	534	31.9	2.71	10.7
47	09	22 Jul: 01	30 Jul: 06	563	39.9	2.43	16.6
48	09	04 Aug:16	13 Aug: 18	514	20.8	2.54	12.6
49	09	17 Aug:08	25 Aug: 19	559	16.5	2.64	11.8
50	09	28 Aug:22	03 Sep: 09	471	12.7	1.26	12.3
51	09	03 Sep:10	08 Sep:03	484	19.3	1.47	8.3
52	09	13 Sep:11	20 Sep:10	460	27.4	1.38	8.2
53	09	20 Sep:11	25 Sep:22	460	15.0	1.38	9.4
54	09	25 Sep:23	07 Oct:22	415	38.9	1.44	9.4
55	09	10 Oct:18	21 Oct: 05	436	48.5	1.68	12.2
56	09	21 Oct:06	04 Nov:09	474	21.3	1.14	11.2
57	09	07 Nov:08	12 Nov:00	442	24.8	1.72	9.7
58	09	18 Nov:17	05 Dec:06	547	20.6	2.88	11.2
59	09	05 Dec:07	12 Dec:04	420	28.8	1.44	9.9
60	09	21 Dec:05	31 Dec:05	427	29.1	1.58	9.4
61	10	11 Jan:01	20 Jan:08	512	33.8	2.91	11.9
62	10	20 Jan:09	29 Jan:18	509	34.2	3.06	15.5
63	10	29 Jan:19	06 Feb:07	559	13.8	2.39	9.8
64	10	16 Feb:14	27 Feb:09	496	09.9	3.11	8.7
65	10	08 Mar:12	22 Mar:10	552	16.2	3.49	9.2
66	10	24 Mar:08	20 Apr:07	783	25.7	7.59	20.2
67	10	28 Apr:16	10 May:08	707	38.7	4.67	18.3
68	10	10 May:09	14 May:13	408	14.0	21.3	8.3
69	10	16 May:19	24 May:16	510	37.2	3.23	13.0
70	10	25 May:03	09 Jun:18	616	26.0	3.31	14.3
71	10	09 Jun:19	23 Jun:09	557	29.1	3.00	10.8
72	10	23 Jun:10	10 Jul:09	683	28.2	3.49	10.0
73	10	10 Jul:10	20 Jul:13	466	41.1	2.09	16.1



74	10	20 Jul:14	12 Aug:14	691	25.0	3.77	17.0
75	10	22 Aug:23	05 Sep:13	693	33.7	4.55	18.8
76	10	05 Sep:14	12 Sep:08	501	19.0	1.85	8.7
77	10	13 Sep:23	23 Sep:00	493	21.1	2.27	10.9
78	10	23 Sep:01	03 Oct:10	620	19.3	2.39	12.2
79	10	04 Oct:17	15 Oct: 00	447	37.4	1.18	13.5
80	10	15 Oct:01	04 Nov:20	658	27.8	3.91	9.9
81	10	10 Nov:13	05 Dec:11	635	29.8	3.44	11.6
82	10	12 Dec:12	22 Dec: 06	654	21.2	4.41	11.5
83	10	06 Jan:16	23 Jan: 16	635	53.1	2.58	13.8
84	11	31 Jan:12	14 Feb:03	647	81.5	5.30	21.0
85	11	14 Feb:09	27 Feb:10	691	75.0	7.08	31.0
86	11	28 Feb:15	09 Mar:18	687	39.0	4.56	14.0
87	11	09 Mar:21	22 Mar: 05	599	24.9	2.88	13.8
88	11	22 Mar:10	27 Mar: 03	516	30.8	2.80	10.4
89	11	31 Mar:20	11 Apr: 05	650	15.9	4.97	15.4
90	11	11 Apr:06	17 Apr: 12	600	53.1	3.49	15.0
91	11	17 Apr:14	28 Apr: 14	555	32.2	3.64	15.9
92	11	28 Apr:15	08 May: 01	703	13.8	7.07	17.3
93	11	09 May:03	21 May: 03	596	32.3	3.86	11.0
94	11	21 May:04	04 Jun:16	752	17.3	10.70	13.0
95	11	04 Jun:18	09 Jun:20	556	56.9	4.10	23.6
96	11	09 Jun:21	29 Jun:16	661	14.9	8.85	10.9
97	11	08 Jul:23	17 Jul:12	708	32.0	5.36	12.8
98	11	17 Jul:13	27 Jul:21	731	09.7	3.58	10.4
99	11	28 Jul:04	04 Aug:04	686	16.2	5.37	14.1
100	11	04 Aug:10	13 Aug:14	632	29.1	10.20	29.4
101	11	13 Aug:19	22 Aug:23	575	28.8	2.65	9.4
102	11	23 Aug:00	31 Aug:22	569	12.3	3.68	8.6
103	11	02 Sep:15	25 Sep:05	652	41.0	6.30	19.3
104	11	25 Sep:07	09 Oct: 14	704	30.5	10.07	34.2
105	11	09 Oct:15	21 Oct: 17	480	19.3	2.45	8.4
106	11	23 Oct:14	29 Oct:05	534	29.3	4.86	24.0
107	11	29 Oct:12	05 Nov:17	436	27.9	1.69	12.6
108	11	06 Nov:00	21 Nov:05	464	22.2	2.62	9.8
109	11	21 Nov:11	07 Dec:05	486	26.0	5.33	17.0
110	11	09 Dec:08	17 Dec:06	491	13.6	3.64	10.7
111	11	18 Dec: 01	27 Dec:06	418	27.2	1.46	9.7

(The peak values of solar plasma/field parameters, solar-wind velocity [V_{\max}], plasma density [N_{\max}], plasma temperature [T_{\max}], and magnetic field [B_{\max}] during each streams

CONCLUSIONS



The velocity of high-speed streams discovered in interplanetary plasma and field data vary greatly. The durations of these streams vary greatly; larger streams might last up to 10 times as long as shorter ones. Singular streams detected in near-Earth space are the result of flows induced by coronal hole(s), coronal mass ejection(s), interplanetary shock(s), and/or their superposed effects. Our investigation into the effect of HSS velocity on GCR-intensity variation revealed that, on average, GCR-intensity drops at the arrival time of the stream with faster streams producing more depressions. Streams of any speed-group, however, are not all GCR effective, nor are all streams of any group equally GCR effective. This reinforces the prior finding that the velocity of the stream is not the only factor determining individual HSS GCR efficiency. From the averaged time profile of the GCR intensity and solar-wind parameters [V , F , σ_F , E , N , and T], we observed that although after the HSS arrival all these solar-wind parameters increase and reach a maximum level, there are time lags between the maxima of these parameters and minima in GCR intensity; however, this time lag is least with V compared with the other solar-wind parameters [F , σ_F , E , N , and T]. Moreover, both during the main and recovery phases, the temporal change in V better matches (in anti-phase) the temporal variation in GCR intensity.

REFERENCES

1. Gopalswamy, N.: 2006, *Astron. Astrophys.* 27, 243.
2. Jian, L., Russel, C.T., Luhmann, J.G., Skoug, R.M.: 2006a, *Solar Phys.*, 239, 393.
3. Sabbah, I., Kudela, K.: 2011, *J. Geophys. Res.* 116, A04103
4. Modzelewska, R., Alania, M.V.: 2012, *Adv. Space Res.* 50, 716.
5. Dumbovic, M., Vrsnak, B., Calagovic, J., Zupar, R.: 2012, *Astron. Astrophys.* 548, A28.
6. Kumar, A., Badruddin: 2014a, *Solar Phys.* 289, 2177.
7. Badruddin: 2006, *Astron. Astrophys.* 27, 209.
8. Gupta, V., Badruddin: 2010, *Solar Phys.* 264, 165.
9. N.M. Wateed et al. (2022) "The impact of various instances of solar wind speed on the fluctuations of cosmic radiation in the solar minima (23, 24, and 25)" Volume 200, November 2022, <https://doi.org/10.1016/j.radphyschem.2022.110134>.
10. Gopalswamy et al (2022) "The Sun and Space Weather" . *Atmosphere* 2022, 13, 1781. <https://doi.org/10.3390/atmos13111781> Received: 17 September 2022 Accepted: 4 October 2022 Published: 28 October 2022.



11. Jacob Oloketuyi et al. (2020) "Responses and Periodic Variations of Cosmic Ray Intensity and Solar Wind Speed to Sunspot Numbers" Volume 2020 | Article ID 3527570 | <https://doi.org/10.1155/2020/3527570>.
12. Arvind Dhurve et al. (2019) "Variations of Cosmic ray intensity in relation to Sunspot Number and Solar Wind Parameters over the period 1996-2019" August 2022 International Journal of Scientific Research in Science and Technology 9(4):418-423 DOI:10.32628/IJSRST229466.
13. Gopalswamy et al. (2017), Coronal flux ropes and their interplanetary counterparts, Journal of Atmospheric and Solar Terrestrial Physics., 84, 212–220.
14. Mittal.N, and U. Narain (2015), On the arrival times of halo coronal mass ejections in the vicinity of the earth, NRIAG Journal of Astronomy and Geophysics, 4, 100–105.
15. Gopalswamy N et al. (2014) Anomalous expansion of coronal mass ejections during solar cycle 24 and its space weather implications. Geophys Res Lett 41:2673–2680.
16. Liou et al. (2014), Global simulation of extremely fast coronal mass ejection on 23 July 2012, Journal of Atmospheric and Solar Terrestrial Physics., 121, 32–41.
17. Rahman.A, et al. (2013), A statistical study on the stand off distances of interplanetary coronal mass ejections, Journal of Atmospheric and Solar Terrestrial Physics., 105-106, 181–190.